

Corresponding Author: *Nitesh Soni*  
 Postal Address:  
*SRF, High Energy Physics Group (Belle Group)*  
*Department of Physics,*  
*Panjab University - Chandigarh - 160014, India*  
 Phone: +91-172-2541741  
 Fax: +91-172-2783336  
 Email: *nitesh@bmail.kek.jp*

## Measurement of Branching Fractions for $B \rightarrow \chi_{c1(2)} K(K^*)$ at Belle

Belle Collaboration

N. Soni<sup>ac</sup>, K. Abe<sup>f</sup>, K. Abe<sup>al</sup>, I. Adachi<sup>f</sup>, H. Aihara<sup>an</sup>,  
 Y. Asano<sup>ar</sup>, V. Aulchenko<sup>a</sup>, T. Aushev<sup>i</sup>, A. M. Bakich<sup>ai</sup>,  
 E. Barberio<sup>q</sup>, I. Bedny<sup>a</sup>, U. Bitenc<sup>j</sup>, I. Bizjak<sup>j</sup>, S. Blyth<sup>t</sup>,  
 A. Bondar<sup>a</sup>, M. Bračko<sup>f,p,j</sup>, T. E. Browder<sup>e</sup>, P. Chang<sup>v</sup>,  
 Y. Chao<sup>v</sup>, A. Chen<sup>t</sup>, K.-F. Chen<sup>v</sup>, B. G. Cheon<sup>b</sup>, R. Chistov<sup>i</sup>,  
 S.-K. Choi<sup>d</sup>, Y. Choi<sup>ah</sup>, A. Chuvikov<sup>ae</sup>, J. Dalseno<sup>q</sup>,  
 M. Danilov<sup>i</sup>, M. Dash<sup>as</sup>, L. Y. Dong<sup>g</sup>, S. Eidelman<sup>a</sup>, Y. Enari<sup>r</sup>,  
 S. Fratina<sup>j</sup>, N. Gabyshev<sup>a</sup>, A. Garmash<sup>ae</sup>, T. Gershon<sup>f</sup>,  
 A. Go<sup>t</sup>, G. Gokhroo<sup>aj</sup>, B. Golob<sup>o,j</sup>, A. Gorišek<sup>j</sup>, J. Haba<sup>f</sup>,  
 T. Hara<sup>ab</sup>, K. Hayasaka<sup>r</sup>, H. Hayashii<sup>s</sup>, M. Hazumi<sup>f</sup>, L. Hinz<sup>n</sup>,  
 Y. Hoshi<sup>al</sup>, S. Hou<sup>t</sup>, W.-S. Hou<sup>v</sup>, T. Iijima<sup>r</sup>, K. Ikado<sup>r</sup>,  
 A. Imoto<sup>s</sup>, A. Ishikawa<sup>f</sup>, R. Itoh<sup>f</sup>, J. H. Kang<sup>at</sup>, J. S. Kang<sup>l</sup>,  
 P. Kapusta<sup>w</sup>, N. Katayama<sup>f</sup>, T. Kawasaki<sup>y</sup>, H. R. Khan<sup>ao</sup>,  
 H. Kichimi<sup>f</sup>, H. J. Kim<sup>m</sup>, S. M. Kim<sup>ah</sup>, S. Korpar<sup>p,j</sup>,  
 P. Križan<sup>o,j</sup>, P. Krokovny<sup>a</sup>, R. Kulasiri<sup>c</sup>, C. C. Kuo<sup>t</sup>,  
 A. Kuzmin<sup>a</sup>, Y.-J. Kwon<sup>at</sup>, T. Lesiak<sup>w</sup>, S.-W. Lin<sup>v</sup>,  
 D. Liventsev<sup>i</sup>, G. Majumder<sup>aj</sup>, F. Mandl<sup>h</sup>, T. Matsumoto<sup>ap</sup>,  
 Y. Mikami<sup>am</sup>, W. Mitaroff<sup>h</sup>, K. Miyabayashi<sup>s</sup>, H. Miyake<sup>ab</sup>,  
 H. Miyata<sup>y</sup>, Y. Miyazaki<sup>r</sup>, R. Mizuk<sup>i</sup>, D. Mohapatra<sup>as</sup>,

T. Nagamine<sup>am</sup>, Z. Natkaniec<sup>w</sup>, S. Nishida<sup>f</sup>, O. Nitoh<sup>aq</sup>,  
S. Ogawa<sup>ak</sup>, T. Ohshima<sup>r</sup>, T. Okabe<sup>r</sup>, S. Okuno<sup>k</sup>, S. L. Olsen<sup>e</sup>,  
Y. Onuki<sup>y</sup>, W. Ostrowicz<sup>w</sup>, H. Ozaki<sup>f</sup>, P. Pakhlov<sup>i</sup>,  
C. W. Park<sup>ah</sup>, R. Pestotnik<sup>j</sup>, M. Peters<sup>e</sup>, L. E. Piilonen<sup>as</sup>,  
Y. Sakai<sup>f</sup>, N. Sato<sup>r</sup>, T. Schietinger<sup>n</sup>, O. Schneider<sup>n</sup>,  
M. E. Sevier<sup>q</sup>, H. Shibuya<sup>ak</sup>, B. Schwartz<sup>a</sup>, V. Sidorov<sup>a</sup>,  
J. B. Singh<sup>ac</sup>, A. Somov<sup>c</sup>, S. Stanič<sup>l</sup>, M. Starič<sup>j</sup>,  
T. Sumiyoshi<sup>ap</sup>, S. Suzuki<sup>af</sup>, S. Y. Suzuki<sup>f</sup>, F. Takasaki<sup>f</sup>,  
K. Tamai<sup>f</sup>, N. Tamura<sup>y</sup>, M. Tanaka<sup>f</sup>, G. N. Taylor<sup>q</sup>,  
Y. Teramoto<sup>aa</sup>, X. C. Tian<sup>ad</sup>, T. Tsuboyama<sup>f</sup>, T. Tsukamoto<sup>f</sup>,  
S. Uehara<sup>f</sup>, K. Ueno<sup>v</sup>, T. Uglov<sup>i</sup>, S. Uno<sup>f</sup>, P. Urquijo<sup>q</sup>,  
G. Varner<sup>e</sup>, S. Villa<sup>n</sup>, C. C. Wang<sup>v</sup>, C. H. Wang<sup>u</sup>,  
Y. Watanabe<sup>ao</sup>, E. Won<sup>ℓ</sup>, Q. L. Xie<sup>g</sup>, A. Yamaguchi<sup>am</sup>,  
Y. Yamashita<sup>x</sup>, M. Yamauchi<sup>f</sup>, J. Ying<sup>ad</sup>, Y. Yuan<sup>g</sup>,  
C. C. Zhang<sup>g</sup>, L. M. Zhang<sup>ag</sup>, Z. P. Zhang<sup>ag</sup>

<sup>a</sup>*Budker Institute of Nuclear Physics, Novosibirsk, Russia*

<sup>b</sup>*Chonnam National University, Kwangju, South Korea*

<sup>c</sup>*University of Cincinnati, Cincinnati, OH, USA*

<sup>d</sup>*Gyeongsang National University, Chinju, South Korea*

<sup>e</sup>*University of Hawaii, Honolulu, HI, USA*

<sup>f</sup>*High Energy Accelerator Research Organization (KEK), Tsukuba, Japan*

<sup>g</sup>*Institute of High Energy Physics, Chinese Academy of Sciences, Beijing, PR China*

<sup>h</sup>*Institute of High Energy Physics, Vienna, Austria*

<sup>i</sup>*Institute for Theoretical and Experimental Physics, Moscow, Russia*

<sup>j</sup>*J. Stefan Institute, Ljubljana, Slovenia*

<sup>k</sup>*Kanagawa University, Yokohama, Japan*

<sup>ℓ</sup>*Korea University, Seoul, South Korea*

<sup>m</sup>*Kyungpook National University, Taegu, South Korea*

<sup>n</sup>*Swiss Federal Institute of Technology of Lausanne, EPFL, Lausanne, Switzerland*

<sup>o</sup>*University of Ljubljana, Ljubljana, Slovenia*

<sup>p</sup>*University of Maribor, Maribor, Slovenia*

<sup>q</sup>*University of Melbourne, Victoria, Australia*

<sup>r</sup>*Nagoya University, Nagoya, Japan*

<sup>s</sup>*Nara Women's University, Nara, Japan*

<sup>t</sup>*National Central University, Chung-li, Taiwan*

- <sup>u</sup>*National United University, Miao Li, Taiwan*
- <sup>v</sup>*Department of Physics, National Taiwan University, Taipei, Taiwan*
- <sup>w</sup>*H. Niewodniczanski Institute of Nuclear Physics, Krakow, Poland*
- <sup>x</sup>*Nippon Dental University, Niigata, Japan*
- <sup>y</sup>*Niigata University, Niigata, Japan*
- <sup>z</sup>*Nova Gorica Polytechnic, Nova Gorica, Slovenia*
- <sup>aa</sup>*Osaka City University, Osaka, Japan*
- <sup>ab</sup>*Osaka University, Osaka, Japan*
- <sup>ac</sup>*Panjab University, Chandigarh, India*
- <sup>ad</sup>*Peking University, Beijing, PR China*
- <sup>ae</sup>*Princeton University, Princeton, NJ, USA*
- <sup>af</sup>*Saga University, Saga, Japan*
- <sup>ag</sup>*University of Science and Technology of China, Hefei, PR China*
- <sup>ah</sup>*Sungkyunkwan University, Suwon, South Korea*
- <sup>ai</sup>*University of Sydney, Sydney, NSW, Australia*
- <sup>aj</sup>*Tata Institute of Fundamental Research, Bombay, India*
- <sup>ak</sup>*Toho University, Funabashi, Japan*
- <sup>al</sup>*Tohoku Gakuin University, Tagajo, Japan*
- <sup>am</sup>*Tohoku University, Sendai, Japan*
- <sup>an</sup>*Department of Physics, University of Tokyo, Tokyo, Japan*
- <sup>ao</sup>*Tokyo Institute of Technology, Tokyo, Japan*
- <sup>ap</sup>*Tokyo Metropolitan University, Tokyo, Japan*
- <sup>aq</sup>*Tokyo University of Agriculture and Technology, Tokyo, Japan*
- <sup>ar</sup>*University of Tsukuba, Tsukuba, Japan*
- <sup>as</sup>*Virginia Polytechnic Institute and State University, Blacksburg, VA, USA*
- <sup>at</sup>*Yonsei University, Seoul, South Korea*

---

## Abstract

We have measured the branching fractions for the exclusive decay modes  $B \rightarrow \chi_{c1(2)}K(K^*)$  using a  $140 \text{ fb}^{-1}$  data sample collected by the Belle detector at the KEKB asymmetric-energy  $e^+e^-$  collider. The measured branching fractions for  $B^+ \rightarrow \chi_{c1}K^+$ ,  $B^0 \rightarrow \chi_{c1}K^0$ ,  $B^0 \rightarrow \chi_{c1}K^{*0}$  and  $B^+ \rightarrow \chi_{c1}K^{*+}$  decay modes are  $(4.5 \pm 0.2 \pm 0.6) \times 10^{-4}$ ,  $(3.5 \pm 0.3 \pm 0.6) \times 10^{-4}$ ,  $(3.0 \pm 0.4 \pm 0.6) \times 10^{-4}$  and  $(4.2 \pm 0.6 \pm 0.7) \times 10^{-4}$ , respectively, where the first error is statistical and the second error is systematic. We do not observe statistically significant signals for the  $B \rightarrow \chi_{c2}K(K^*)$  decay modes and set upper limits at the 90% confidence level. We also study the helicity distribution for  $B \rightarrow \chi_{c1}K^*$  decay mode and show that the

longitudinal polarization component is dominant.

*Keywords:* B-meson, Charmonium, Branching Fractions, Polarization

*PACS:* 13.25.Hw, 11.30.Er

---

## 1 Introduction

Decays of  $B$  mesons to two-body final states including a charmonium meson have played a crucial role in the observation of  $CP$ -violation in the  $B$  system [1]. These decay modes also provide a sensitive laboratory for studying strong interaction (QCD) effects in a heavy meson system. One widely used approximation to handle QCD effects in heavy meson decays is “factorization”, where it is assumed that the participating quarks form hadrons without subsequent transfer of quantum numbers between the hadrons. In the factorization limit, two-body  $B$  decays of the type  $B \rightarrow \chi_{c0}X$  and  $\chi_{c2}X$  are suppressed by angular momentum and vector current conservation [2,3]. Belle has reported the observation of exclusive  $B^\pm \rightarrow \chi_{c0}K^\pm$  [4] and the measurement of inclusive  $B \rightarrow \chi_{c2}X$  decays [5]. Rescattering of  $D_s^*D^*$  has been proposed as an alternative explanation of the large decay rate for  $B \rightarrow \chi_{c0}K$  [6]<sup>2</sup>. This mechanism also predicts a branching fraction for  $B \rightarrow \chi_{c2}K$  comparable to that for  $B \rightarrow \chi_{c0}K$ . Therefore either factorization or rescattering must be tested by another  $B$  decay measurement. The measurement of  $B \rightarrow \chi_{c1}K^*$  and  $B \rightarrow \chi_{c2}K^*$  will give important information because the former is allowed and the latter is inhibited in the factorization picture; both  $\chi_{c1}$  and  $\chi_{c2}$  can be reconstructed from the common final state of  $\gamma J/\psi$ . In this paper, we report a study of exclusive decays  $B \rightarrow \chi_{c1(2)}K(K^*)$  for both charged and neutral  $B$  mesons.

These measurements are based on a  $140 \text{ fb}^{-1}$  data sample which contains 152 million  $B\bar{B}$  pairs, collected with the Belle detector [7] at the KEKB asymmetric-energy  $e^+e^-$  (3.5 GeV on 8 GeV) collider [8] operating at the  $\Upsilon(4S)$  resonance.

---

<sup>1</sup> on leave from Nova Gorica Polytechnic, Nova Gorica, Slovenia

<sup>2</sup> Throughout this paper, when a mode is quoted the inclusion of charge conjugate mode is implied.

## 2 Belle Detector

The Belle detector is a large-solid-angle magnetic spectrometer. Closest to the interaction point is a three-layer silicon vertex detector (SVD), followed by a 50-layer central drift chamber (CDC), an array of aerogel threshold Čerenkov counters (ACC), a barrel-like arrangement of time-of-flight (TOF) scintillation counters, and an electromagnetic calorimeter (ECL) comprised of CsI(Tl) crystals. These subdetectors are located inside a superconducting solenoid coil that provides a 1.5 T magnetic field. An iron flux-return located outside of the coil is instrumented to detect  $K_L^0$  mesons and to identify muons (KLM). The detector is described in detail elsewhere [7].

## 3 Event selection

Events with  $B$ -meson candidates are selected first by applying general hadronic event selection criteria. These include a requirement on charged tracks (at least three of them should originate from the event vertex consistent with the interaction region), a requirement on the reconstructed center-of-mass (CM) energy ( $E^{CM} > 0.2\sqrt{s}$ , where  $\sqrt{s}$  is the total CM energy), a requirement on the longitudinal ( $z$ -direction) component of the reconstructed CM momentum with respect to the beam direction ( $|p_z^{CM}| < 0.5\sqrt{s}/c$ ) and a requirement on the total ECL energy ( $0.1\sqrt{s} < E_{ECL}^{CM} < 0.8\sqrt{s}$  with at least two energy clusters). To suppress continuum background, we also require that the ratio of the second and zeroth Fox-Wolfram moments [9] be less than 0.5. To remove charged particle tracks that are poorly measured or do not come from the interaction region, we require  $dz < 5$  cm for all tracks other than those identified as decay daughters of  $K_S^0$ , where  $dz$  is the track's closest approach to the interaction point along the beam direction.

## 4 $\chi_{c1(2)}$ meson candidates

The  $\chi_{c1(2)}$  meson states are reconstructed *via* the decay mode  $\chi_{c1(2)} \rightarrow \gamma J/\psi$  with  $J/\psi \rightarrow \ell^+ \ell^-$ , where  $\ell$  is muon or electron. For muon tracks, identification is based on track penetration depth and the hit pattern in the KLM system [10]. Electron tracks are identified by a combination of  $dE/dx$  from the CDC,  $E/p$  ( $E$  is the energy deposited in the ECL and  $p$  is the momentum measured by the SVD and the CDC) and shower shape in the ECL [11]. In order to recover di-electron events in which one or both electrons have radiated a photon, the four momenta of all photons within 0.05 radian of the  $e^+$  or  $e^-$  directions are included in the invariant mass calculation. The invariant

mass windows are  $-0.06$  ( $-0.15$ )  $\text{GeV}/c^2 \leq M_{\ell^+\ell^-} - M_{J/\psi} \leq 0.036$   $\text{GeV}/c^2$  to select  $J/\psi$  candidates in the  $\mu^+\mu^-(e^+e^-)$  channels; these intervals are asymmetric in order to include part of the radiative tails. Vertex and mass-constrained kinematic fits are then performed for selected  $J/\psi$  candidates to improve the momentum resolution. The  $\chi_c$  states are reconstructed by combining a  $J/\psi$  candidate with momentum below 2  $\text{GeV}/c$  in the CM frame with all photons of energy greater than 0.060  $\text{GeV}$  in the laboratory frame; we veto photons that, when combined with another photon in the event, satisfies  $0.110$   $\text{GeV}/c^2 \leq m_{\gamma\gamma} \leq 0.150$   $\text{GeV}/c^2$  to suppress photons from  $\pi^0$  decays. The  $\chi_{c1(2)}$  candidates are selected by requiring the mass difference ( $M_{\ell^+\ell^-\gamma} - M_{\ell^+\ell^-}$ ) to lie between 0.385  $\text{GeV}/c^2$  and 0.431  $\text{GeV}/c^2$  for  $\chi_{c1}$ , and between 0.436  $\text{GeV}/c^2$  and 0.482  $\text{GeV}/c^2$  for  $\chi_{c2}$ . Mass-constrained fits are applied to all selected  $\chi_{c1}$  and  $\chi_{c2}$  candidates.

## 5 $K$ or $K^*$ candidates

The  $K^{*0}$  and  $K^{*+}$  candidates are reconstructed from four decay modes:  $K^{*0} \rightarrow K^+\pi^-$  or  $K_S^0\pi^0$ , and  $K^{*+} \rightarrow K^+\pi^0$  or  $K_S^0\pi^+$ . The kaon likelihood ratio for a track is defined as  $\mathcal{L}(K/\pi) = \mathcal{L}(K)/(\mathcal{L}(K) + \mathcal{L}(\pi))$ . Charged kaons are identified by requiring  $\mathcal{L}(K/\pi)$  to be  $> 0.6$ . The kaon and pion likelihoods ( $\mathcal{L}(K)$  and  $\mathcal{L}(\pi)$ ) are obtained by combining measurements from the TOF and the CDC ( $dE/dx$ ) with hit information from the ACC. Tracks which are not identified as either a kaon or a lepton are treated as charged pion candidates. In the reconstruction of the decay mode  $B^+ \rightarrow \chi_{c1(2)}K^+$ , all well-measured tracks other than the ones from the  $J/\psi$  are considered to be kaon candidates. In order to eliminate the systematic error from particle identification and to retain high efficiency, no particle identification cut for kaons is applied. The  $K_S^0$  candidates are reconstructed from pairs of oppositely charged pions. The  $\pi^+\pi^-$  pair is required to be displaced from the interaction point (IP) by a minimum transverse distance of 0.22 cm for high momentum ( $> 1.5$   $\text{GeV}/c$ ) candidates and 0.08 cm for those with momentum less than 1.5  $\text{GeV}/c$ . The direction of the pion pair momentum must agree with the direction defined by the IP and the vertex displacement within 0.03 rad for high momentum candidates ( $> 1.5$   $\text{GeV}/c$ ), within 0.1 rad for candidates having momentum between 1.5  $\text{GeV}/c$  to 0.5  $\text{GeV}/c$  and within 0.3 rad for the remaining low momentum candidates. The invariant mass of the  $\pi^+\pi^-$  pair candidate is required to satisfy  $-0.482$   $\text{GeV}/c^2 \leq M_{\pi^+\pi^-} \leq 0.514$   $\text{GeV}/c^2$ . The  $\pi^0$  candidates are reconstructed from pairs of photons with energies greater than 0.060  $\text{GeV}$ . The  $\pi^0$  candidates are required to have invariant mass  $0.120$   $\text{GeV}/c^2 < M_{\gamma\gamma} < 0.150$   $\text{GeV}/c^2$ . A mass-constrained fit is performed to obtain the momentum of the  $\pi^0$ . To reduce the background from slow pions, we require the  $\pi^0$  momentum to be greater than 0.2  $\text{GeV}/c$  in the

CM frame.

## 6 $B$ meson reconstruction

We reconstruct  $B$  mesons by combining a  $\chi_{c1}$  or  $\chi_{c2}$  candidate with a charged or neutral  $K(K^*)$  candidate. We form two independent kinematic variables: the beam constrained mass  $M_{bc} \equiv \sqrt{(E_{\text{beam}}/c^2)^2 - ((\vec{p}_{\chi_{c1(2)}} + \vec{p}_{K(K^*)})/c)^2}$ , and  $\Delta E \equiv (E_{\chi_{c1(2)}} + E_{K(K^*)}) - E_{\text{beam}}$ , where  $E_{\text{beam}}$  is the beam energy, and  $p_{\chi_{c1(2)}}$ ,  $E_{\chi_{c1(2)}}$ ,  $p_{K(K^*)}$  and  $E_{K(K^*)}$  are momenta and energies in the CM frame of the  $\chi_c$  states and the  $K(K^*)$  mesons, respectively. The  $B$ -meson signal window is defined as  $5.27 \text{ GeV}/c^2 \leq M_{bc} \leq 5.29 \text{ GeV}/c^2$  for all channels and the ranges for  $\Delta E$  are  $\pm 0.025 \text{ GeV}$  for  $B \rightarrow \chi_{c1(2)} K(K_S^0)$ , and  $\pm 0.040 \text{ GeV}$  for  $B \rightarrow \chi_{c1(2)} K^*(K^+\pi^- \text{ or } K_S^0\pi^+)$ . A larger range ( $-0.050 \text{ GeV} \leq \Delta E \leq 0.030 \text{ GeV}$ ) is used for  $B \rightarrow \chi_{c1(2)} K^{*+}(K^+\pi^0 \text{ or } K_S^0\pi^0)$  to accommodate the wider  $\Delta E$  distribution that results from energy leakage in the calorimeter for  $\pi^0$  modes.

## 7 Signal yield and background estimation

To study the sources of background, we use 5.5 million  $B \rightarrow J/\psi$  inclusive Monte Carlo events generated using the event generator EvtGen [12] and a GEANT3-based program [13] to simulate the Belle detector response. Based on this study, the backgrounds for  $B \rightarrow \chi_{c1(2)} K(K_S^0)$  decay modes can be categorized as  $J/\psi$  inclusive and feed-across backgrounds. The  $J/\psi$  inclusive background occurs due to a true  $J/\psi$  candidate accidentally combining with a unrelated  $\gamma$  to fake a  $\chi_{c1(2)}$ . Feed-across background is due to one mode being reconstructed as a different mode because of the similarity in event kinematics. For  $B \rightarrow \chi_{c1(2)} K^*$  decay modes, there is an additional background due to non-resonant decays of  $B$  mesons i.e.  $B \rightarrow \chi_{c1(2)} K\pi$ . Non-resonant background peaks at the same place as signal in the  $M_{bc}$  and  $\Delta E$  distributions, but does not peak in the  $K\pi$ -mass distribution. We thus extract the number of signal events from a fit to the  $M_{bc}$  distribution for  $B \rightarrow \chi_{c1(2)} K(K_S^0)$  decay modes but use the  $K\pi$ -mass distribution for  $B \rightarrow \chi_{c1(2)} K^*$  decay modes. Each component of background has been estimated separately as discussed below. The  $J/\psi$  inclusive background is modeled by the sidebands in the  $(M_{\ell^+\ell^-\gamma} - M_{\ell^+\ell^-})$  mass distribution and scaled according to the fitted area of the background under the  $\chi_{c1(2)}$  signal region. The sidebands are defined as  $0.2 \text{ GeV}/c^2$  to  $0.3 \text{ GeV}/c^2$  and  $0.55 \text{ GeV}/c^2$  to  $0.60 \text{ GeV}/c^2$  in the  $(M_{\ell^+\ell^-\gamma} - M_{\ell^+\ell^-})$  mass distribution. This model includes a contribution from the combinatorial  $\ell^+\ell^-$  background under the  $J/\psi$  peak (“fake  $J/\psi$  candidates”), which is not present in the  $J/\psi$  inclusive Monte Carlo sample; this component forms about 5% of

the  $J/\psi$  inclusive background. As a systematic check, the  $J/\psi$  inclusive Monte Carlo has also been used to model the  $J/\psi$  inclusive background. The small difference in the fit between the two models has been included in the systematic error.

To represent the feed-across background for each decay mode  $i$ , due to other  $\chi_{c1(2)}K(K^*)$  modes  $j \neq i$ , we take the appropriate Monte Carlo histograms and normalize them according to the signal yields observed in the modes  $j$ . The total feed-across background for mode  $i$  is then fixed in the fit. The fitting procedure for all twelve  $\chi_{c1(2)}K(K^*)$  modes is repeated, using the signal yields from the previous iteration as input, until we find a stable result.

The non-resonant background shape is obtained from the  $J/\psi$  inclusive Monte Carlo sample. Due to low statistics and the similar shapes of  $J/\psi$  inclusive and non-resonant background, it is not possible to float simultaneously the normalizations of both backgrounds in the fit to data. We have little knowledge about the amount of non-resonant background, so when fitting the  $K\pi$ -mass distribution the normalization of the  $J/\psi$  inclusive background is fixed while it is floated for non-resonant background.

The  $M_{bc}$  distributions for  $B \rightarrow \chi_{c1(2)}K(K_S^0)$  decay modes are fitted with a Gaussian to describe the signal region. The width and mean value of the Gaussian are fixed in the fit using MC values that are calibrated by the  $B^+ \rightarrow \chi_{c1}K^+$  decay mode in data because this mode has the highest statistics among the decay modes considered. The background shapes for the  $J/\psi$  inclusive and feed-across backgrounds have been modeled as discussed above. The normalization parameter for the feed-across background histogram is fixed while it is floated for the  $J/\psi$  inclusive background histogram. Figure 1 displays the fit to the  $M_{bc}$  distributions for the (a)  $B^+ \rightarrow \chi_{c1}K^+$ , (b)  $B^+ \rightarrow \chi_{c2}K^+$ , (c)  $B^0 \rightarrow \chi_{c1}K_S^0$ , and (d)  $B^0 \rightarrow \chi_{c2}K_S^0$  decay modes. The signal yields extracted from these distributions are listed in Table 1. For the  $B \rightarrow \chi_{c2}K(K_S^0)$  mode, no statistically significant signal is seen. As a check, the signal yields have also been obtained by fitting the  $\Delta E$  distributions for the  $B \rightarrow \chi_{c1(2)}K(K_S^0)$  decay modes and are found to be consistent with the signal yields obtained from the fits to the  $M_{bc}$  distributions.

A relativistic P-wave Breit-Wigner function is used to fit the  $K^*(892)$  signal region in the  $K\pi$ -mass distributions for the  $B \rightarrow \chi_{c1(2)}K^*$  decay modes. For  $K^*(892)$ , the width and peak of the P-wave Breit-Wigner function are found to be consistent between data and MC in the  $B \rightarrow J/\psi K^*(892)$  decay modes [14]; therefore, those parameters are fixed to the PDG values in the fit [15]. The shapes of the  $J/\psi$  inclusive, feed-across and non-resonant backgrounds are modeled as explained previously. There may be some structure in the  $K_2^*(1430)$  region in the  $K\pi$ -mass distributions for the  $B \rightarrow \chi_{c1(2)}K^*$  decay modes. To accomodate this possibility we have included a relativistic



D-wave Breit-Wigner function in the fits to the  $K\pi$ -mass distributions. The mean and width of the D-wave Breit-Wigner function are fixed to the nominal PDG values. Fig. 2 shows the fits to the  $K\pi$ -mass distribution for the (a)  $B^0 \rightarrow \chi_{c1} K^{*0}(K^+\pi^-)$ , (b)  $B^0 \rightarrow \chi_{c1} K^{*0}(K_S^0\pi^0)$ , (c)  $B^+ \rightarrow \chi_{c1} K^{*+}(K^+\pi^0)$ , and (d)  $B^+ \rightarrow \chi_{c1} K^{*+}(K_S^0\pi^+)$  decay modes. The fits to the  $K\pi$ -mass distributions for (a)  $B^0 \rightarrow \chi_{c2} K^{*0}(K^+\pi^-)$ , (b)  $B^0 \rightarrow \chi_{c2} K^{*0}(K_S^0\pi^0)$ , (c)  $B^+ \rightarrow \chi_{c2} K^{*+}(K^+\pi^0)$ , and (d)  $B^+ \rightarrow \chi_{c2} K^{*+}(K_S^0\pi^+)$  decay modes are presented in Fig. 3. The signal yields extracted from these distributions are listed in Table 1. For the  $B^0 \rightarrow \chi_{c1} K^{*0}(K_S^0\pi^0)$  and  $B \rightarrow \chi_{c2} K^*$  decay modes, no statistically significant signals are seen. The signal yields have also been checked by fitting the  $M_{bc}$  and  $\Delta E$  distributions for the  $B \rightarrow \chi_{c1(2)} K^*$  decay modes and are found to be consistent with the signal yields obtained from the fit to the  $K\pi$ -mass distributions.

## 8 Helicity study for $B \rightarrow \chi_{c1} K^*$ decays

A  $P \rightarrow VV$  decay may include three possible polarization amplitudes: two transverse and one longitudinal. The contributions of these amplitudes can be obtained from the helicity distribution of the  $K^*$  ( $\cos\theta_{K^*}$ ) where  $\theta_{K^*}$  is defined as the angle between the  $K^*$  momentum and the direction opposite to the  $B$  momentum in the  $K^*$  rest frame. The transverse polarization amplitudes have a  $\sin^2\theta_{K^*}$  dependence while the longitudinal amplitude has a  $\cos^2\theta_{K^*}$  dependence. We have analysed the helicity distributions for different  $K\pi$ -mass regions. The efficiency-corrected  $\cos\theta_{K^*}$  distribution for the signal region ( $0.821 < M_{K\pi} < 0.971$  GeV/c<sup>2</sup>) is fitted with the function  $f(\cos\theta_{K^*}) = A + B\cos\theta_{K^*} + C\cos^2\theta_{K^*}$ . The fitted value of  $B$  ( $3.4 \pm 24.6$ ) is consistent with zero, which shows that there is no asymmetric term present in the signal region. The helicity distribution for the background ( $M_{K\pi} < 0.8$  GeV/c<sup>2</sup>) is flat except for a peak in the last bin due to the  $J/\psi$  inclusive background (Fig. 4(a)); this distribution for the signal region is significantly different as shown in Fig. 4(b). The efficiency-corrected  $\cos\theta_{K^*}$  distributions for the signal and background regions are fitted with the function  $f(\cos\theta_{K^*}) = A + 3B\cos^2\theta_{K^*}$ . From the fitted values of  $A$  and  $B$  for the two regions we have estimated the longitudinal polarization of the  $K^*$ , which is calculated as  $\eta = |(A_L/A_{\text{total}})|^2 = (B' + A'/3)/(A' + B')$ , where  $A_L$  and  $A_{\text{total}}$  are the amplitudes for longitudinal and total polarization, and  $A'$ ,  $B'$  are the background subtracted fitted values of  $A$ ,  $B$  for the signal region, respectively. We obtain  $\eta = 0.87 \pm 0.09$ . The fit difference with or without inclusion of the last peaking bin of the  $\cos\theta_{K^*}$  distribution for the background region is small and the error assigned to  $\eta$  takes into account this effect. From the value of  $\eta$  we conclude that the  $B \rightarrow \chi_{c1} K^*$  decay is dominated by longitudinal polarization with a lower limit for the longitudinal polarization of 0.72 at the

90% confidence level. This result for longitudinal polarization in  $B \rightarrow \chi_{c1} K^*$  decay is consistent with the factorization model. According to factorization in the Standard Model the longitudinal polarization fraction in decays of  $B$  mesons to vector-vector final states is close to unity [16]. However, this is not consistent with observations of the decay  $B \rightarrow J/\psi K^*$  [14].

## 9 Measurement of branching fractions

The branching fraction for each  $B \rightarrow \chi_{c1(2)} K(K^*)$  decay mode is estimated by dividing the observed signal yield by the reconstruction efficiency, the number of  $B\bar{B}$  events in the data sample and the daughter branching fractions. We have used the daughter branching fractions published in PDG 2004 [15]. Equal production of neutral and charged  $B$  meson pairs in  $\Upsilon(4S)$  decay is assumed. Reconstruction efficiencies are estimated by applying the same selection criteria to 20,000 signal Monte Carlo events. The efficiencies for each final state are shown in Table 1. Here, the branching fraction of  $K^0 \rightarrow K_S^0 \rightarrow \pi^+\pi^-$  is not included in the efficiency calculation. In the fits to data, the width of the  $\chi_{c2}$  is constrained to be 10% larger than the width of the  $\chi_{c1}$  as expected from Monte Carlo simulation and the photon resolution. The effect of this assumption is included in the systematic errors. To calculate upper limits (U.L.), we add the statistical and systematic errors in quadrature, and assume that the combined error behaves as a Gaussian. We then follow the prescription of Feldman and Cousins [17]. The branching fractions are summarized in Table 1. The first errors are statistical and the second errors are systematic. The statistical significance ( $\Sigma$ ) of the signal in terms of number of standard deviations is calculated as  $\sqrt{-2\ln(\mathcal{L}_0/\mathcal{L}_{max})}$ , where  $\mathcal{L}_{max}$  and  $\mathcal{L}_0$  denote the maximum likelihood with the nominal signal yield and with the signal yield fixed at zero, respectively. If a decay mode is reconstructed in two final states, e.g.  $B^+ \rightarrow \chi_{c1} K^{*+}(K_S^0 \pi^+)$  and  $B^+ \rightarrow \chi_{c1} K^{*+}(K^+ \pi^0)$ , the two branching fraction measurements are averaged, weighted by the statistical and systematic errors. A comparison between our measurement and those due to BaBar [18,19] is also shown in Table 3.

## 10 Systematic uncertainties

The sources of systematic uncertainty are summarized in Table 2. The uncertainty on the tracking efficiency is estimated to be 1.5% for  $e$  and  $\pi$  tracks, and 1.1% for  $\mu$  and  $K$  tracks. The pion tracks from  $K_S^0$  decay are from a displaced vertex and thus have a larger systematic error; we include 3.5% per track uncertainty for pion tracks from  $K_S^0$  decays. The errors on electron and

muon identification are 1.6% and 2.2%, respectively. The kaon identification error is estimated to be 2%.

Uncertainties on  $\gamma$  and  $\pi^0$  reconstruction efficiency are 2% and 4%, respectively. The uncertainty in the  $K_S^0$  selection efficiency is checked by comparing yields for a sample of high momentum  $K_S^0 \rightarrow \pi^+\pi^-$  decays before and after applying the  $K_S^0$  selection criteria. The efficiency difference between data and Monte Carlo simulation is less than 1.0%.

All modes have a systematic uncertainty due to  $\chi_{c1(2)} \rightarrow \gamma J/\psi$  and  $J/\psi \rightarrow \ell^+\ell^-$  branching fractions; the uncertainties for these modes are taken from the PDG [15] and added in quadrature.

To estimate the possible systematic errors due to interference between the signal and background, we fit the  $K\pi$ -mass distribution to a function which assumes a coherent background contribution. We define this function as

$$F(m_{K\pi}) = |\sqrt{N_s}S(m_{K\pi}) + \sqrt{(N_b a_c)}e^{i\phi}B(m_{K\pi})|^2 + N_b(1 - a_c)B^2(m_{K\pi}) \quad (1)$$

where

$$S(m_{K\pi}) = \frac{m_{K^*}\Gamma(m_{K\pi})}{(m_{K\pi}^2 - m_{K^*}^2) + im_{K^*}\Gamma(m_{K\pi})} \quad (2)$$

is a relativistic P-wave Breit-Wigner function with  $m_{K^*} = 892 \text{ MeV}/c^2$ ,  $B(m_{K\pi})$  is the phase space background function,  $N_s$  and  $N_b$  are the numbers of events for signal and background, respectively, and  $a_c$  is the fraction of coherent background with phase  $\phi$  relative to the signal. The maximum value of the coherent background fraction is taken from the helicity analysis to be  $a_c = 0.6$ . From this fit we find that the maximum difference in the signal yield due to the possible interference term is 15%. This difference has been included as a systematic error.

The yield measurements are taken from fits where the mean and width of the signal shape are fixed. The corresponding uncertainty is estimated by varying the means and widths in turn by  $\pm 1\sigma$ , and repeating the fit. The percentage change in the signal yield is presented in Table 2. The difference between two background fitting models (i.e. using the  $J/\psi$  inclusive background shapes from data or from the  $J/\psi$  inclusive Monte Carlo) has also been included as a systematic error listed as background error (“Bkg. Error”) in Table 2.

For the  $\chi_{c1}$  modes, the error on the efficiency correction due to the  $\chi_{c1}$  width is based on the uncertainty of the fitted width in data. For the  $\chi_{c2}$  modes, there

are additional effects due to the assumptions in the fit:  $\chi_{c2} : \chi_{c1} = 1.1 : 1$  (estimated by an alternative fit where  $\chi_{c1}$  and  $\chi_{c2}$  widths float independently). The resulting errors have been estimated and listed as efficiency correction (“Eff. Corr.”) in Table 2.

The uncertainty on the number of  $B\bar{B}$  events, which is common to all modes, is 1%; this is negligible compared to the other systematic errors.

## 11 Conclusion

We have measured the branching fractions for the  $B \rightarrow \chi_{c1(2)}K(K^*)$  decay modes using 152 million  $B\bar{B}$  events. Although inclusive  $\chi_{c2}$  signals in  $B$  decay have been observed [5], we do not find any significant signals for exclusive two-body  $B \rightarrow \chi_{c2}K(K^*)$  decay modes. The branching fractions for  $B \rightarrow \chi_{c1}K(K^*)$  decay modes are of the order of 10% of the  $\psi$  inclusive branching fractions [5]. We see no statistically significant signals for  $B \rightarrow \chi_{c2}K(K^*)$  and set limits on branching fractions at the 90% confidence level which are an order of magnitude smaller than those for  $B \rightarrow \chi_{c1}K(K^*)$ . The helicity distribution for the  $B \rightarrow \chi_{c1}K^*$  decay mode shows that the longitudinal polarization component is dominant.

## 12 Acknowledgments

We thank the KEKB group for the excellent operation of the accelerator, the KEK cryogenics group for the efficient operation of the solenoid, and the KEK computer group and the National Institute of Informatics for valuable computing and Super-SINET network support. We acknowledge support from the Ministry of Education, Culture, Sports, Science, and Technology of Japan and the Japan Society for the Promotion of Science; the Australian Research Council and the Australian Department of Education, Science and Training; the National Science Foundation of China under contract No. 10175071; the Department of Science and Technology of India; the BK21 program of the Ministry of Education of Korea and the CHEP SRC program of the Korea Science and Engineering Foundation; the Polish State Committee for Scientific Research under contract No. 2P03B 01324; the Ministry of Science and Technology of the Russian Federation; the Ministry of Higher Education, Science and Technology of the Republic of Slovenia; the Swiss National Science Foundation; the National Science Council and the Ministry of Education of Taiwan; and the U.S. Department of Energy.

## References

- [1] K. Abe *et al.* (Belle Collaboration), Phys. Rev. Lett. **86**, 2509 (2001); **87**, 091802 (2001); Phys. Rev. **D 66**, 071102(R) (2002); **66**, 032007 (2002); B. Aubert *et al.*, (BaBar Collaboration) Phys. Rev. Lett. **86**, 2515 (2001); **87**, 091801 (2001); Phys. Rev. **D 66**, 032003 (2002); Phys. Rev. Lett. **89**, 201802 (2002).
- [2] M. Suzuki, Phys. Rev. **D 66**, 037503 (2002).
- [3] M. Bauer, B. Stech, M. Wirbel, Z. Phys. **C 34**, 103 (1987).
- [4] K.Abe, *et al.* (Belle Collaboration), Phys. Rev. Lett. **88**, 031802 (2002).
- [5] K.Abe, *et al.* (Belle Collaboration), Phys. Rev. Lett. **89**, 011803 (2002).
- [6] P. Colangelo, F.De Fazio and T.N. Pham, Phys. Lett. **B 542**, 71 (2002); hep-ph/0207061.
- [7] A. Abashian *et al.* (Belle Collaboration), Nucl. Instrum. Methods Phys. Res., Sect. **A 479**, 117 (2002).
- [8] S. Kurokawa and E. Kikutani, Nucl. Instrum. Methods Phys. Res., Sect. **A 499**, 1 (2003).
- [9] G. Fox and S. Wolfram, Phys. Rev. Lett., **41** 1581 (1978).
- [10] A. Abashian *et al.*, Nucl. Instrum. Methods Phys. Res., Sect. **A 491** 69 (2002).
- [11] K. Hanagaki *et al.*, Nucl. Instrum. Methods Phys. Res., Sect. **A 485** 490 (2002).
- [12] We use the EvtGen  $B$ -meson decay generator developed by the CLEO and the BaBar Collaborations, see: <http://www.slac.stanford.edu/~lange/EvtGen/>.
- [13] CERN program library long writeup W5013, CERN, (1993).
- [14] K. Abe *et al.*, (Belle Collaboration), Phys. Lett. **B 538**, 11 (2002).
- [15] Particle Data Group, S. Eidelman *et al.*, Phys. Lett. **B 592**, 1 (2004).
- [16] A.L. Kagan, Phys. Lett. **B 601**, 151 (2004).
- [17] G.J. Feldman and R.D. Cousins, Phys. Rev. **D 57**, 3873 (1998).
- [18] B. Aubert *et al.*, (BaBar Collaboration), Phys. Rev. Lett. **94**, 171801 (2005), hep-ex/0501061.
- [19] B. Aubert *et al.*, (BaBar Collaboration), Phys. Rev. Lett. **94**, 141801 (2005), hep-ex/0408036.

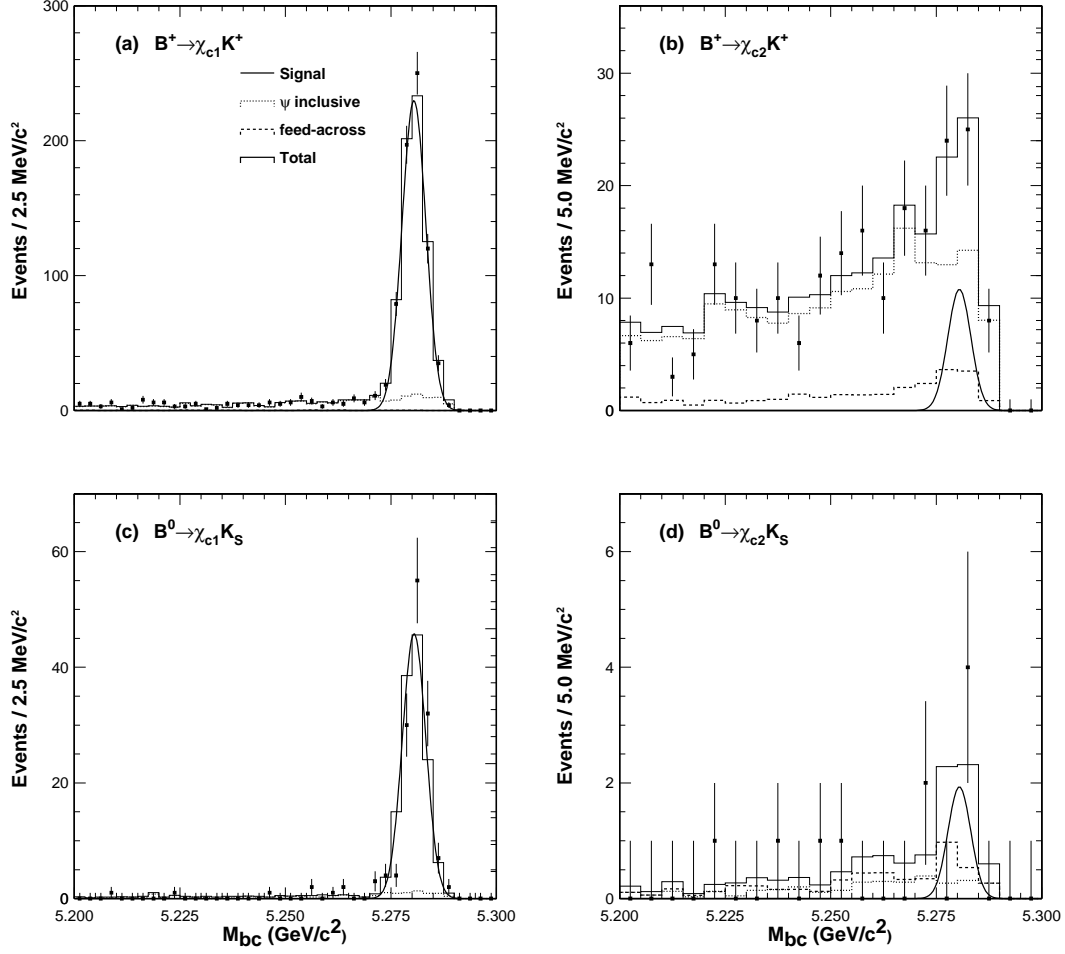


Fig. 1. The  $M_{bc}$  distribution for (a)  $B^+ \rightarrow \chi_{c1} K^+$ , (b)  $B^+ \rightarrow \chi_{c2} K^+$ , (c)  $B^0 \rightarrow \chi_{c1} K_S^0$  and (d)  $B^0 \rightarrow \chi_{c2} K_S^0$  decay modes, respectively, together with results of the fit for the signal region and contributions due to feed-across and  $J/\psi$  inclusive backgrounds.

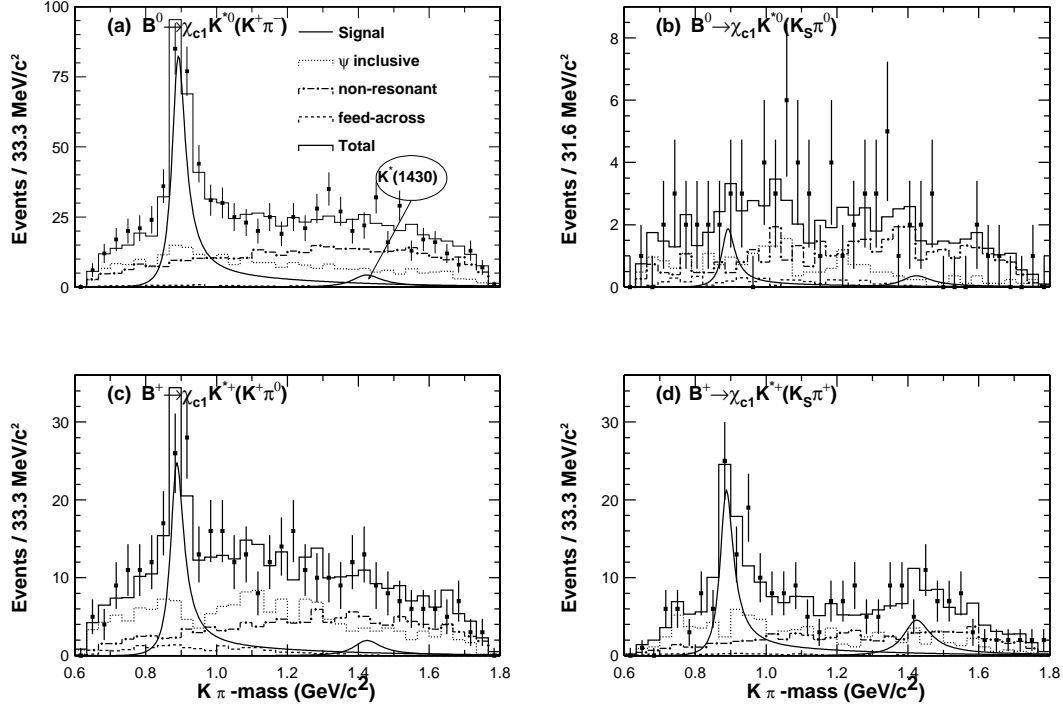


Fig. 2. The  $K\pi$ -mass distribution for (a)  $B^0 \rightarrow \chi_{c1} K^{*0} (K^+ \pi^-)$ , (b)  $B^0 \rightarrow \chi_{c1} K^{*0} (K_S^0 \pi^0)$ , (c)  $B^+ \rightarrow \chi_{c1} K^{*+} (K^+ \pi^0)$ , and (d)  $B^+ \rightarrow \chi_{c1} K^{*+} (K_S^0 \pi^+)$  decay modes, respectively, together with results from the fit to  $K^*$  signals and contributions of backgrounds due to  $J/\psi$  inclusive, non-resonant and feed-across backgrounds.

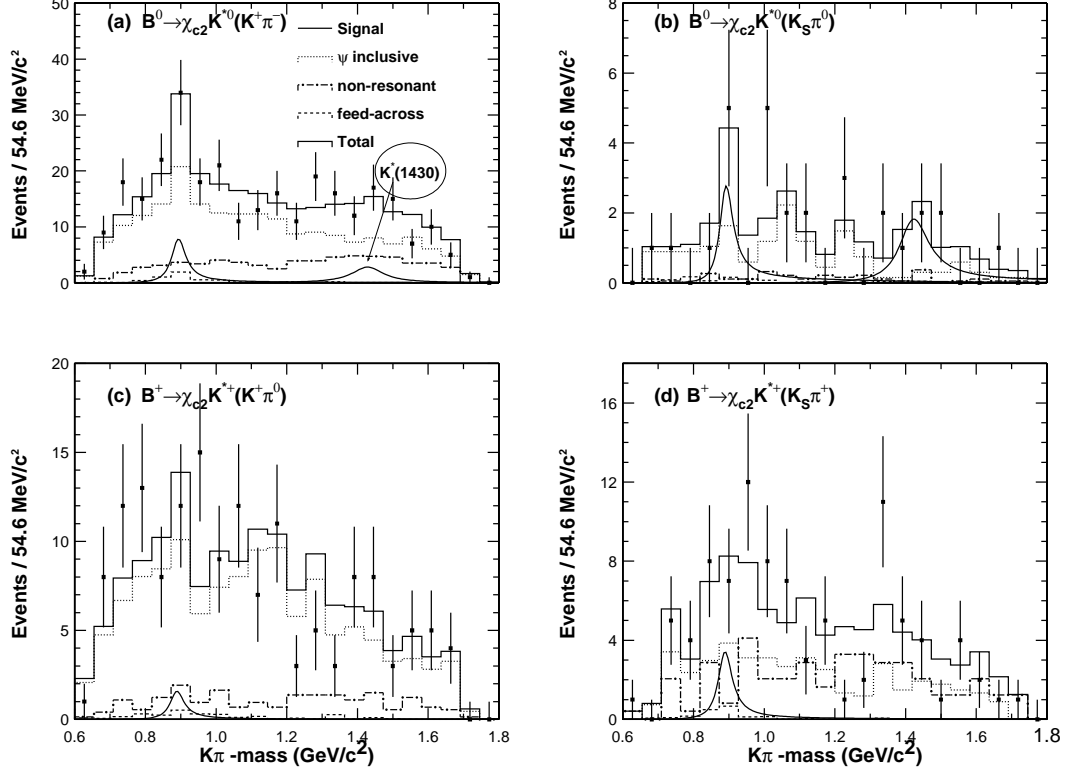


Fig. 3. The  $K\pi$ -mass distribution for (a)  $B^0 \rightarrow \chi_{c2} K^{*0}(K^+\pi^-)$ , (b)  $B^0 \rightarrow \chi_{c2} K^{*0}(K_S^0\pi^0)$ , (c)  $B^+ \rightarrow \chi_{c2} K^{*+}(K^+\pi^0)$ , and (d)  $B^+ \rightarrow \chi_{c2} K^{*+}(K_S^0\pi^+)$  decay modes, respectively, together with results from fit to  $K^*$  signals and contributions of backgrounds due to  $J/\psi$  inclusive, non-resonant and feed-across backgrounds.

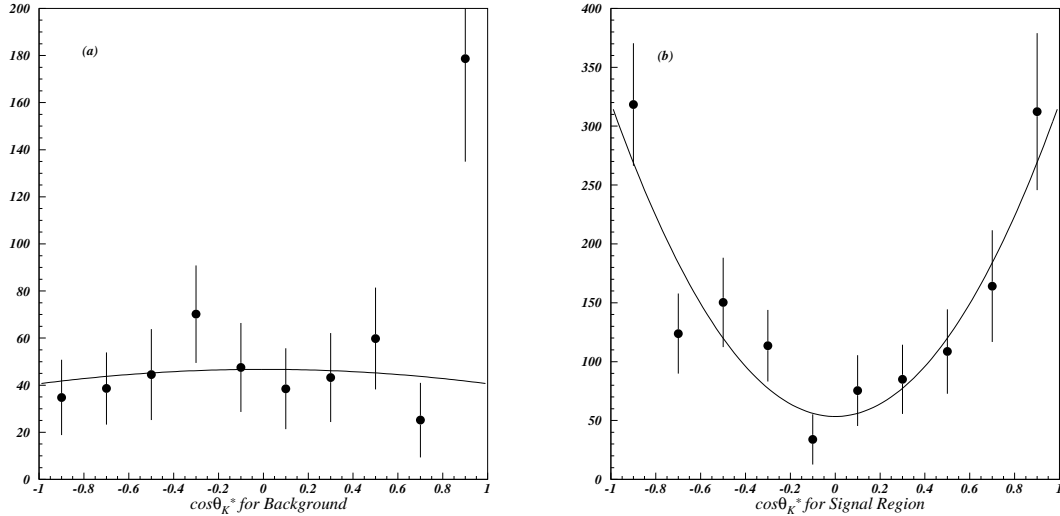


Fig. 4. The efficiency-corrected  $\cos \theta_{K^*}$  distributions for  $B^0 \rightarrow \chi_{c1} K^{*0}(K^+\pi^-)$  decay mode fitted with  $f(\cos \theta_{K^*}) = A + 3B \cos^2 \theta_{K^*}$  function for (a) background region ( $M_{K\pi} < 0.8 \text{ GeV}/c^2$ ) and (b) signal region ( $0.821 < M_{K\pi} < 0.971 \text{ GeV}/c^2$ ).



Table 1

The summary of the estimated branching fractions for  $B \rightarrow \chi_{c1(2)}K(K^*)$  decay modes. First (second) quoted error is statistical (systematic). Here  $K^0$  is reconstructed through the decay chain  $K^0 \rightarrow K_S^0 \rightarrow \pi^+\pi^-$ .

Mode	Efficiency $\mathcal{E}(\%)$	Yield	Br. Fraction ( $\mathcal{B}$ ) $\times 10^{-4}$	U.L.(90% C.L.) $\times 10^{-4}$	Sign. ( $\Sigma$ )
$B^+ \rightarrow \chi_{c1}K^+$	25.4	$645.7 \pm 26.9$	$4.49 \pm 0.19 \pm 0.59$		37.4
$B^0 \rightarrow \chi_{c1}K^0$	18.5	$127.0 \pm 11.8$	$3.53 \pm 0.33 \pm 0.58$		15.3
$B^0 \rightarrow \chi_{c1}K^{*0}(K^+\pi^-)$	17.4	$209.9 \pm 22.7$	$3.22 \pm 0.35 \pm 0.71$		12.1
$B^0 \rightarrow \chi_{c1}K^{*0}(K^0\pi^0)$	4.2	$5.0 \pm 4.8$	$1.84 \pm 1.76 \pm 0.96$		1.1
$B^0 \rightarrow \chi_{c1}K^{*0}$			$3.03 \pm 0.38 \pm 0.63$		
$B^+ \rightarrow \chi_{c1}K^{*+}(K^0\pi^+)$	11.4	$53.6 \pm 11.1$	$3.66 \pm 0.76 \pm 1.07$		6.9
$B^+ \rightarrow \chi_{c1}K^{*+}(K^+\pi^0)$	7.0	$62.6 \pm 13.2$	$4.79 \pm 1.01 \pm 0.99$		6.0
$B^+ \rightarrow \chi_{c1}K^{*+}$			$4.18 \pm 0.62 \pm 0.74$		
$B^+ \rightarrow \chi_{c2}K^+$	24.9	$14.8 \pm 7.7$	$0.16 \pm 0.09 \pm 0.03$	0.28	2.1
$B^0 \rightarrow \chi_{c2}K^0$	18.3	$2.6 \pm 2.1$	$0.11 \pm 0.09 \pm 0.03$	0.27	1.6
$B^0 \rightarrow \chi_{c2}K^{*0}(K^+\pi^-)$	16.5	$11.7 \pm 9.4$	$0.30 \pm 0.24 \pm 0.12$		1.3
$B^0 \rightarrow \chi_{c2}K^{*0}(K^0\pi^0)$	4.6	$4.3 \pm 3.5$	$2.26 \pm 1.84 \pm 0.63$		1.6
$B^0 \rightarrow \chi_{c2}K^{*0}$			$0.34 \pm 0.24 \pm 0.12$	0.76	
$B^+ \rightarrow \chi_{c2}K^{*+}(K^0\pi^+)$	11.2	$5.2 \pm 5.4$	$0.57 \pm 0.59 \pm 0.14$		1.1
$B^+ \rightarrow \chi_{c2}K^{*+}(K^+\pi^0)$	7.3	$2.5 \pm 7.2$	$0.29 \pm 0.83 \pm 0.31$		0.3
$B^+ \rightarrow \chi_{c2}K^{*+}$			$0.48 \pm 0.48 \pm 0.14$	1.30	

Table 2  
Summary of the multiplicative systematic errors in terms of number of events (ev.) and percent (%) for all modes. Here the columns list the individual systematic error components: Trk., Lep., and Had. are those associated with tracking, and lepton & hadron efficiencies;  $\gamma/\pi^0$  refers to  $\gamma$  and  $\pi^0$  reconstruction;  $K_S^0$  refers to the  $K_S^0$  selection efficiency; B.F. refers to the secondary branching fractions; Phase Interference refers to the interference between  $K^*$  signal and non-resonant  $K\pi$  background; Fit. Para. lists sensitivity to the fit parameters; Bkg. Errors refers to different fitting models for the  $J/\psi$  inclusive background; and Eff. Corr. lists errors associated with the efficiency correction.

Modes	Efficiency Uncertainty					B.F.	Phase Interference	Fit Para.( $\pm 1\sigma$ )	Total		Bkg. Errors	Eff. Corr.	Total	
	Trk.	Lep.	Had.	$\gamma/\pi^0$	$K_S^0$				Multiplicative					
	%	%	%	%	%				%	(ev.)			(ev.)	(ev.)
$B^+ \rightarrow \chi_{c1} K^+$	3.7	3.8	—	2	—	10.6	—	$< 1$	12.0	$\pm 77.5$	$\pm 4.9$	$\pm 1.9$	$\pm 84.3$	13.1
$B^0 \rightarrow \chi_{c1} K^0$	9.6	3.8	—	2	1	10.6	—	$< 1$	15.0	$\pm 19.1$	$\pm 1.2$	$\pm 0.4$	$\pm 20.7$	16.3
$\overline{B}^0 \rightarrow \chi_{c1} K^{*0}(K^+\pi^-)$	5.2	3.8	1.9	2	—	10.6	15.0	$< 1$	19.7	$\pm 41.1$	$\pm 4.2$	$\pm 0.6$	$\pm 46.3$	22.1
$B^0 \rightarrow \chi_{c1} K^{*0}(K^0\pi^0)$	9.6	3.8	—	4.5	1	10.6	15.0	$< 1$	21.5	$\pm 1.1$	$\pm 1.5$	$\pm 0.0$	$\pm 2.6$	52.0
$B^+ \rightarrow \chi_{c1} K^{*+}(K^0\pi^+)$	11.1	3.8	0.8	2	1	10.6	15.0	$< 1$	21.9	$\pm 11.7$	$\pm 3.8$	$\pm 0.2$	$\pm 15.7$	29.3
$B^+ \rightarrow \chi_{c1} K^{*+}(K^+\pi^0)$	3.7	3.8	1.1	4.5	—	10.6	15.0	$< 1$	19.7	$\pm 12.3$	$\pm 0.5$	$\pm 0.2$	$\pm 13.0$	20.8
$B^+ \rightarrow \chi_{c2} K^+$	3.7	3.8	—	2	—	8.6	—	$< 1$	10.3	$\pm 1.5$	$\pm 1.2$	$\pm 0.3$	$\pm 3.0$	20.3
$B^0 \rightarrow \chi_{c2} K^0$	9.6	3.8	—	2	1	8.6	—	$< 1$	13.6	$\pm 0.4$	$\pm 0.2$	$\pm 0.1$	$\pm 0.7$	26.9
$B^0 \rightarrow \chi_{c2} K^{*0}(K^+\pi^-)$	5.2	3.8	1.9	2	—	8.6	15.0	$< 1$	18.7	$\pm 2.2$	$\pm 1.8$	$\pm 0.2$	$\pm 4.2$	35.9
$B^0 \rightarrow \chi_{c2} K^{*0}(K^0\pi^0)$	9.6	3.8	—	4.5	1	8.6	15.0	$< 1$	20.6	$\pm 0.9$	$\pm 0.2$	$\pm 0.1$	$\pm 1.2$	27.9
$B^+ \rightarrow \chi_{c2} K^{*+}(K^0\pi^+)$	11.1	3.8	0.8	2	1	8.6	15.0	3.8	21.4	$\pm 1.1$	$\pm 0.1$	$\pm 0.1$	$\pm 1.3$	25.0
$B^+ \rightarrow \chi_{c2} K^{*+}(K^+\pi^0)$	3.7	3.8	1.1	4.5	—	8.6	15.0	8.0	20.3	$\pm 0.5$	$\pm 2.1$	$\pm 0.1$	$\pm 2.7$	108.0

Table 3

Comparison between this measurement and those due to BaBar [18,19]. First (second) quoted error is statistical (systematic).

Mode	Belle		BaBar	
	Br. Fraction $\times 10^{-4}$	U.L.(90% C.L.) $\times 10^{-4}$	Br. Fraction $\times 10^{-4}$	U.L.(90% C.L.) $\times 10^{-4}$
$B^+ \rightarrow \chi_{c1} K^+$	$4.49 \pm 0.19 \pm 0.59$		$5.79 \pm 0.26 \pm 0.65$	
$B^0 \rightarrow \chi_{c1} K^0$	$3.53 \pm 0.33 \pm 0.58$		$4.53 \pm 0.41 \pm 0.51$	
$B^0 \rightarrow \chi_{c1} K^{*0}$	$3.03 \pm 0.38 \pm 0.63$		$3.27 \pm 0.42 \pm 0.64$	
$B^+ \rightarrow \chi_{c1} K^{*+}$	$4.18 \pm 0.62 \pm 0.74$		$2.94 \pm 0.95 \pm 0.98$	
$B^+ \rightarrow \chi_{c2} K^+$	$0.16 \pm 0.09 \pm 0.03$	0.28	$0.09 \pm 0.10 \pm 0.11$	0.30
$B^0 \rightarrow \chi_{c2} K^0$	$0.11 \pm 0.09 \pm 0.03$	0.27	$0.21 \pm 0.11 \pm 0.13$	0.41
$B^0 \rightarrow \chi_{c2} K^{*0}$	$0.30 \pm 0.24 \pm 0.12$	0.76	$0.14 \pm 0.11 \pm 0.14$	0.36
$B^+ \rightarrow \chi_{c2} K^{*+}$	$0.48 \pm 0.48 \pm 0.14$	1.30	$-0.15 \pm 0.05 \pm 0.14$	0.12